Faraday Discussions

Accepted Manuscript

This manuscript will be presented and discussed at a forthcoming Faraday Discussion meeting. All delegates can contribute to the discussion which will be included in the final volume.

Register now to attend! Full details of all upcoming meetings: http://rsc.li/fd-upcoming-meetings

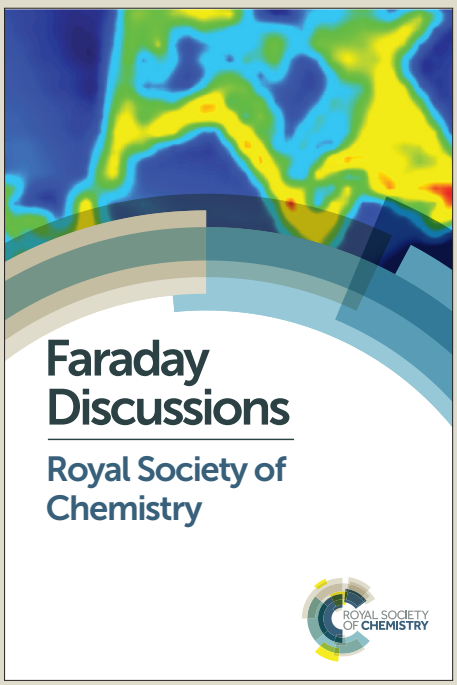

This is an *Accepted Manuscript*, which has been through the Royal Society of Chemistry peer review process and has been accepted for publication.

Accepted Manuscripts are published online shortly after acceptance, before technical editing, formatting and proof reading. Using this free service, authors can make their results available to the community, in citable form, before we publish the edited article. We will replace this *Accepted Manuscript* with the edited and formatted *Advance Article* as soon as it is available.

You can find more information about *Accepted Manuscripts* in the Information for Authors.

Please note that technical editing may introduce minor changes to the text and/or graphics, which may alter content. The journal's standard Terms & Conditions and the Ethical guidelines still apply. In no event shall the Royal Society of Chemistry be held responsible for any errors or omissions in this *Accepted Manuscript* or any consequences arising from the use of any information it contains.

ROYAL SOCIETY OF CHEMISTRY

www.rsc.org/faraday_d

Journal Name

ARTICLE

Received 00th January 20xx,
Accepted 00th January 20xx

DOI: 10.1039/x0xx00000x

www.rsc.org/

Quantitative structural information from single-molecule FRET

M. Beckers,[a] F. Drechsler,[a] T. Eilert,[a] J. Nagy[a] and J. Michaelis[a]

Abstract

Single-molecule studies can be used to study biological processes directly and in real-time. In particular the fluorescent energy transfer between reporter dye molecules attached to specific sites on macromolecular complexes can be used to infer distance information. When several measurements are combined the information can be used to determine the position and conformation of certain domains with respect to the complex. However, data analysis schemes that include all experimental uncertainties are highly complex, and the outcome depends on assumptions about the state of the dye molecules. Here, we present a new analysis algorithm using Bayesian parameter estimation based on Markov Chain Monte Carlo sampling and Parallel Tempering termed Fast-NPS that can analyse large smFRET networks in relatively short time and yields the position of the dye molecules together with their respective uncertainties. Moreover, we show what effects different assumptions about the dye molecules have on the outcome. We discuss the possibilites and pitfalls in structure determination based on smFRET using experimental data for an archaeal transcription pre-initiation complex, whose architecture has recently been unravelled by smFRET measurements.

[a] *Biophysics Institute, Ulm University, 89081 Ulm, Germany.*
† Footnotes relating to the title and/or authors should appear here.
Electronic Supplementary Information (ESI) available: [details of any supplementary information available should be included here]. See DOI: 10.1039/x0xx00000x

Introduction

Structural biology has in the last decades revolutionised our understanding of many important cellular functions, such as transcription,[1] translation,[2] nucleic acid translocases,[3] or motor proteins such as myosin,[4] among many others. While these studies provide (nearly) atomic models for these complex machineries, in order to mechanistically understand protein function, dynamic information is required as well. Here, in particular single-molecule methods have become the method of choice,[5] since they provide the means to observe the action of a single enzyme across time. In particular, when attaching a pair of dye molecules at specific locations and measuring the Förster resonance energy transfer between them (smFRET), information about conformational changes becomes accessible. While already quite early on, FRET has been termed a *molecular ruler*,[6] obtaining quantitative information from FRET measurements has proven to be quite difficult.[7]

One idea used to obtain structural information from smFRET measurements was to determine an unknown position using a triangulation, or more correctly a trilateration approach.[8-10] However, while measuring smFRET efficiencies can be done quite accurately if care is taken to perform the required corrections,[4,11] rather larger uncertainties arise due to the relative orientation of the dye molecules, resulting in an uncertainty of κ^2 and thus an uncertainty in the Förster distance.[12] Moreover, the quantum yield of the donor could be sensitive to local changes and thus increase the experimental uncertainty in distance determination.[13] Another important factor when using smFRET data to determine distances is the fact that dye molecules are attached via flexible linkers and can be located anywhere inside their so-called accessible volume (AV).[14]

In order to arrive at quantitative structural information we have developed the Nano-Positioning System (NPS) [14,15] and have applied it to obtain insight into transcription elongation[14,16] and transcription initiation complexes.[17-19] NPS uses Bayesian parameter estimation together with a static model of the dye linker, assuming that the linker takes up a specific, however unknown conformation. Quantum yield variations are accounted for by performing a molecule-wise correction of the quantum yield, and the relative orientation of the dye molecules is either modelled by a Förster radius prior computed using the measured anisotropies of donor and acceptor,[14] or by determining the dye orientations explicitly, followed by a marginalisation to the pure position

information.[15] NPS computes the three-dimensional probability distribution for each dye position, i.e. the marginalised posterior, which is best visualised by the smallest volume enclosing a certain probability, i.e. the credible volume. Depending on the number of measurements used, as well as on the geometry of the problem, the 1σ error can be as low as 3Å,[14] but more typical values are on the order of 10-20Å.[19] While at this resolution important structural insight into transcription elongation and transcription initiation was obtained,[14,16-20] in order to achieve such a resolution, large networks of FRET measurements were analysed globally, resulting in computation times of several weeks.

More recently, another related approach has been published, termed FRET-restrained positioning and screening (FPS).[21] FPS treats the dye molecules attached to the macromolecule differently. First, it is assumed that the dye molecules are free to re-orient on the time-scale of the fluorescent lifetime, implying $\kappa^2=2/3$. The second assumption is that due to its flexible linker each dye molecule is free to move within its AV. Furthermore it is assumed that the dye occupies each position within its AV for an equally long time, such that its position can be represented by a mean position (MP). However, in order to correctly account for the R^6-dependence of the energy transfer, the distance of mean positions R_{MP} is converted into the FRET-weighted donor-acceptor distance R_{DA} using a polynomial fit. The obtained quantitative smFRET distance constraints are then used for arranging several parts of a biological complex into a rigid-body docking scenario, thus allowing smFRET to be used for structure determination. In benchmark studies, the FPS-derived structure of the DNA primer-template bound to the HIV-1 reverse transcriptase yielded root mean square deviations as low as 0.5Å compared to the X-ray structure, and the structure of an ssDNA overhang was determined with a precision of 2.9Å.[21] While for several steps in the analysis a rigorous error estimate was performed,[22] the precision was not determined from the posterior shape and size but rather using a bootstrapping approach.

A related, less stringent approach for smFRET-restrained structure determination had been published earlier.[23] Here, molecular dynamics (MD) simulations were used for determining the dye position attached via a flexible linker; however, no correction for the R^6-dependence of FRET was applied and no rigorous error estimate was performed.

Here, we present an improved NPS analysis method, termed Fast-NPS,‡ which uses Markov Chain Monte Carlo (MCMC) sampling which has been sped up via Parallel Tempering, shortening computation times by two orders of magnitude. Moreover, we have added the capability to test different models for the respective dye molecules, thus enabling us to compare the results of different approaches. We test the new NPS scheme on recently published data of the archaeal transcription initiation complex.[19]

Results

Effective MCMC sampling of large smFRET networks. In NPS, the information from an arbitrarily large set of measurements between satellite dye molecules (SDM), attached to known positions of a macromolecule, and antenna dye molecules (ADM), attached to unknown positions is analysed globally using Bayesian parameter estimation yielding the posterior for the set of all dye molecules:[15]

$$p(\{\boldsymbol{x_i},\boldsymbol{\Omega_i}\}|\{E_{ij}\},\{A_{ij}\},I) = p(\{\boldsymbol{x_i},\boldsymbol{\Omega_i}\}|I) * p(\{E_{ij}\},\{A_{ij}\}|(\{\boldsymbol{x_i},\boldsymbol{\Omega_i}\},I)/Z\,, \quad (1)$$

where $p(\{\boldsymbol{x_i},\boldsymbol{\Omega_i}\}|I)$ is the prior which encodes the information before the measurement, and $p(\{E_{ij}\},\{A_{ij}\}|(\{\boldsymbol{x_i},\boldsymbol{\Omega_i}\},I)$ is the likelihood which describes the expected data given the set of dye positions $\boldsymbol{x_i}$ and average transition dipole orientations $\boldsymbol{\Omega_i}$. The evidence is denoted by Z, which for a given set of data is a constant and will in the following be treated as unity for simplicity. The measured FRET efficiency between molecules *i* and *j* is denoted by E_{ij}, and A_{ij} denotes the measured FRET anisotropy between the respective molecules.[15] The latter type of measurement is not required but improves the accuracy of the NPS analysis. Now, in order to obtain the probability distribution of the position x_i of one single ADM *i* one marginalises the posterior by integration:[15]

$$p\left(\{\boldsymbol{x}_i\}\middle|\{E_{ij}\},\{A_{ij}\},I\right) = \int d\{\boldsymbol{x}_{j\neq i},\boldsymbol{\Omega}_i\}\, p\left(\{\boldsymbol{x}_j,\boldsymbol{\Omega}_j\}\middle|\{E_{ij}\},\{A_{ij}\},I\right)$$

In our original publication a nested sampling algorithm was used for computing the posterior. While reliable, we experienced excessively large computation times on the order of weeks for the large smFRET networks used to study transcription complexes.

We therefore decided to sample the posterior using an MCMC algorithm and employed Metropolis-within-Gibbs sampling, an efficient way for computing posteriors in Bayesian parameter estimation.[24]

In order to further speed up the analysis and to ensure that even posteriors consisting of several well-separated maxima are faithfully represented, we also employed Parallel Tempering, sometimes also referred to as replica exchange or Metropolis-coupled-MCMC.[25,26] It is a powerful technique to overcome several problems regarding simple MCMC algorithms, including multimodality and poor mixing (i.e. bad exploration of the state space). Parallel Tempering is also often used as an enhanced sampling method for MD simulations; in contrast, here it is employed to achieve better mixing and to guarantee that all local maxima of the posterior are found. The idea behind parallel tempering is the simulation of the same system at different virtual temperatures – the higher the temperature, the lower the energy barriers in the respective potential energy landscape. Thus, a Markov chain is more likely to cross an energy barrier at higher temperatures and this way the trajectory can jump between different maxima. Replicas are run in parallel at different temperatures and after a certain number of steps of each, swaps of the complete states are proposed between different replicas, i.e. temperatures, and accepted or rejected using a Metropolis-

Hastings criterion. These swaps force the lowest-temperature chain, i.e. the system of interest, to explore the energy landscape more widely. Thus, multimodalities are more likely to be found.

In our implementation the temperature spacing of different replicas follows a geometric ladder,[27] i.e. the inverse temperatures of the replicas are given by $K_0 = 1$, and $K_i=K_{i-1}*0.4$ for $i = 1, \ldots, n$; the scale of 0.4 having been chosen experimentally for optimal performance.

In order to speed up the analysis even further, we used different adaptation algorithms of our MCMC sampler, details of which will be published elsewhere. The Fast-NPS implementation allowed us to analyse large smFRET networks using standard office computers on the order of hours, yielding one million samples to describe the posterior.

Archaeal transcription initiation complexes. One important question in the field of transcription is the architecture and dynamics of multi-component transcription initiation complexes. We have recently studied the architecture of the pre-initiation complex (PIC) of *M. Janaschii*, consisting of archaeal RNA polymerase, transcription factors TBP, TFB, TFE and promoter DNA, using smFRET and the NPS system.[19] Using SDMs attached on various subunits of the polymerase and ADMs attached to the promoter DNA, TBP, TFE and TFB (Figure 1), we assembled over 70 different complexes. Each of these complexes was labelled with a single smFRET pair attached to well definded positions. The information from all these measurements was used to build a model of the general architecture of the PIC. Here, we will use this smFRET network as a test-scenario for the new NPS algorithm. While NPS analysis using nested sampling took several weeks, using MCMC extended by parallel tempering we were able to compute the posterior on a time-scale of hours (Figure 2B). Overall there is very good agreement between the computed credible volumes between NPS using nested sampling and MCMC. However, the faster computation times allowed us to test the influence of several key assumptions in NPS on the overall precision and accuracy of the model.

Comparison of different dye models in NPS. While smFRET experiments allow one to obtain structural information about a particular macromolecule, the assumptions of how the dye molecule is modelled will impact the results (Figure 3). In the original NPS analysis scheme we chose a fairly conservative model of the dye molecules: They were thought to reside in one particular location within their AV (static model), and the orientation of the transition dipole moment fluctuates within a cone about the mean orientation with the cone opening angle determined by the fluorescence anisotropy (*classic model*, Figure 3B). Both these assumptions are conservative in the sense that they lead to large uncertainties and as a result the resulting credible volumes are fairly large. In the following we want to relax these conditions and monitor the effect on the credible volume size and position. We expect that under less conservative assumptions, the determined credible volumes will shrink, however, we would like to develop criteria which help understanding whether a particular assumption is justified, or if it may cause inconsistencies in the analysis.

First, we consider the situation that for all measurements, both donor and acceptor molecules are sufficiently free to rotate so that the orientations average dynamically across the lifetime of the fluorescent state, and thus $\kappa^2=2/3$ can be used for all smFRET measurements (Figure 3C). We termed this situation the *isotropic orientation NPS* (*iso model*). In the new Fast-NPS program we have included the possibility to use an isotropic orientation for all dye molecules. In order to test the performance of the Fast-NPS and to compare the results of this more restrictive *iso model* to the *classic model*, we again use the smFRET scenario of the archaeal PIC and compute posteriors for all ADMs (Figure 2B). By comparing the credible volumes, it becomes evident that the assumption of isotropic orientation drastically reduces the experimental uncertainty and as a result leads to much smaller credible volumes, with the average volume being about 40 times smaller than for the *classic model* (Figure 4).

Next, we wanted to test the effect of the static linker model used in NPS. While in the NPS system, a static model is used, others have argued that the linker is better described by a dynamic averaging over all possible positions within the AV.[21] This results in a mean position at the center of the AV. Therefore, in addition to using the dynamically averaged orientation scheme, we also implemented the possibility of dynamic position averaging (*meanpos-iso model*, Figure 2D). To account for the averaging we use a polynomial conversion of R_{MP} to R_{DA}. While strictly speaking the published values of the polynomial fit are only valid for the situation of dye molecules attached internally to DNA, we found that changing the shape of the AV had only small effects on the resulting polynomial. Considering the fact that the polynomial will result in changes only for very small distances, the use of an exact, specific polynomial is not likely to dramatically alter the results. We again analysed the archaeal PIC smFRET network with model 3 (Figure 2C). Comparison of the *iso model* and the *meanpos-iso model* shows that the additional assumption of a fixed mean position leads to a further reduction of credible volumes by a factor of 3 (Figure 4). When comparing to model 1, one should note that also the mean position is a possibility within the static model (even though a static position of the linker pointing into free space seems artificial); however, in NPS the mean position would then lead to slightly altered smFRET values compared to the dynamically averaged position, due to the R^6-dependence of FRET. While this difference is very small for low FRET efficiencies, it cannot be neglected for situations where donor and acceptor molecules are quite close, resulting in FRET efficiencies of around 80% or higher.

While MD simulations have indicated that the mean position of the AV volume is a good model for non-interacting dye molecules attached to linear DNA molecules,[21] when dyes are attached to

proteins the situation might be more complicated because the dye molecule could interact with regions on the protein surface or simply stick to small cavities created by surface residues. In order to account for these effects we have tested another model, where we use the dynamical averaging of dipole orientations, and the dynamical averaging of positions within the AV, while allowing the freedom that the center of mass is no longer at the center of the AV but can take an arbitrary position within the AV (*var-meanpos-iso model*, Figure 3E). To include this in our analysis scheme we do not impose a fixed mean position but let the sampler find the most likely mean position. Again, we account for the dynamic position averaging by using the polynomial conversion of R_{MP} to R_{DA}. We again analysed the archaeal PIC smFRET network (Figure 2D). The computed credible volumes have a size comparable to those of the *iso model* (Figure 4). However, the positions of the credible volumes are shifted compared to those of the *iso model* and the *meanpos-iso model*.

In a last scenario, we wanted to investigate the effect of dynamic averaging of different positions for a situation where the dye molecule is not completely free to rotate (*var-meanpos model*, Figure 3F). Such a situation could occur for example if the dye molecule binds reversibly to several different positions on the protein surface. When applying this model to the archaeal PIC smFRET network, we find credible volumes which are comparable in size to those of Model 1 (Figure 4), albeit at slightly shifted positions.

Influence of dye molecules with high fluorescence anisotropy on network analysis. From the comparison of the credible volumes of Models 1-5 we find that the largest effect on the size of the credible volume is the isotropic averaging over all possible dye orientations. The linker position and whether one considers one static or many dynamically averaged positions only has a minor effect on the size of the credible volumes. This is in accordance with our previous observation that the localisation accuracy of NPS is mainly dependent on our precise knowledge of the orientation of the dye molecules.[15] While the isotropic averaging of dye orientations is a good assumption when the FRET anisotropy is fairly low, high FRET anisotropies could lead to substantial errors in the analysis.[7] We therefore wanted to test whether in the analysed smFRET network, isotropic orientation averaging could lead not only to a reduction in uncertainty but also to a shifted position of the credible volume. For such a case one could argue that the unjustified use of $\kappa^2=2/3$ could lead to wrong interpretations of the smFRET results.

In order to test this hypothesis we investigated the overlap of credible volumes of different models. To this end, we computed credible volumes at increasing probability to test at which confidence level the credible volumes of different models begin to overlap by at least one voxel (voxel size in our analysis was 8Å^3). This analysis was done for all ADMs. Since one can expect that the isotropic orientation averaging is a good hypothesis when the fluorescence anisotropy is low, but might fail for higher fluorescence anisotropies, we plotted the described threshold confidence level as a function of fluorescence anisotropy (Figure 5).

We compared both, the situation of a variable dynamic mean position (*var-meanpos-iso model*), as well as that of a fixed dynamic mean position (*meanpos-iso model*) to the *var-meanpos* model. For all ADMs the overlap for *var-meanpos-iso model* occurred earlier than that for the *meanpos-iso model*. In fact, in this case the volumes overlapped for all ADMs before 68% credibility was reached, indicating that the two models are consistent with each other. When comparing the *meanpos-iso model* with the *var-meanpos model*, the first overlap occurs at values as high as 98 %, suggesting that the assumptions of the *meanpos-iso model* are very unlikely for some dyes (e.g. nt(-24) or TBP), since the assumed ADM state in the *meanpos-iso model* is also possible in the *var-meanpos model*. At first sight, the level at which overlap occurs does not clearly correlate with fluorescence anisotropy, i.e. small observed anisotropies do not necessarily result in overlaps at low confidence levels. However, one has to keep in mind that analysis is done in a global scheme. Therefore, one ADM for which the $\kappa^2=2/3$ approximation or the fixed dynamically averaged mean position assumption is not valid could have detrimental effects also on the localisation of another ADM, in particular if direct measurements between the two ADMs are included. In the smFRET scenario at hand, this becomes quite evident for the analysis of the positions -24, -30 and -37 on the non-template strand. All these ADMs have rather low fluorescence anisotropies, yet overlap occurs only at high confidence levels when comparing the *meanpos-iso* with the *var-meanpos model*.

We plotted arrows indicating the shift in the credible level at which overlap occurs upon the introduction of a fixed mean position (switch from the *var-meanpos-iso* to the *meanpos-iso model*). In view of the argument above we used green arrows for describing localisations that used measurements to TBP and/or TFB, and black arrows for all other localisations. Green arrows are generally much longer than black arrows suggesting that especially the assumption of a fixed mean position with respect to the accessible volume (AV) might not be valid here. Therefore, when using both the $\kappa^2=2/3$ assumption and the fixed mean position, overlap occurs only at extremely high values, suggesting that the analysis model is not consistent with the experimentally observed data. In order to test whether the samples from ADMs used in smFRET measurements to TFB or TBP show a significant difference compared to the other ADMs, a two-sample Wilcoxon-Man-Whitney test was performed at 95 % confidence level upon the credible volumes, testing the percentage at which the first overlap occurred. This was done for the model comparison *meanpos-iso* versus *var-meanpos* (blue dots in Figure 5), as especially there, the difference between high and low anisotropies was significant. All in all this led to the rejection of the null-hypothesis that the two sets of samples are from the same distribution, which can be taken as evidence for a significant difference of the medians of the two distributions. We interpret this as an inconsistency in the analysis of the *meanpos-iso model*.

Conclusions

We have exhibited a novel implementation of the NPS analysis scheme based on MCMC sampling and parallel tempering, decreasing the time needed for the analysis by ≈2 orders of magnitude. The new algorithm works very reliably and the resulting credible volumes are virtually identical to those published earlier. With this new analysis scheme we also implemented the possibility to change the model of the conformational behaviour of dye molecules. In particular we tested effects of isotropic orientation averaging as well as dynamic position averaging about the center of the accessible volume or about another unknown position within the accessible volume.

We find that the isotropic orientation assumption reduces the size of the credible volumes dramatically. Moreover, when combined with a dynamic position averaging about the center of the accessible volume, the size of the credible volumes becomes so small that the precision of smFRET-based structure determination becomes comparable to what can be achieved by high resolution x-ray crystallography, as has been previously used in FRET-restrained position sensing.[21] However, careful analysis of the overlap of the credible volumes of different dye molecule prior showed that the isotropic orientation averaging can also lead to inconsistencies in the analysis. Especially when combined with the stringent assumptions of the *meanpos-iso model*, this would result in false structural information. Thus great caution has to be used when applying these assumptions. One can test the resulting models by bootstrapping approaches, given sufficient amount of data. However, it might be beneficial to use other dye priors such as the ones presented here instead..

Acknowledgements

We thank Adam Muschielok for insightful comments and discussion regarding NPS, as well as different sampling schemes. We also want to thank Timo Breßmer for help with the programming at initial phases of this project.

Figure 1: ***Schematic of the NPS analysis of the archaeal PIC****. (A) Cartoon depicting the archaeal PIC complex, including DNA (tDNA in dark grey, ntDNA in light grey) and transcription factors (TBP in pink, TFB in green and TFE in yellow). Labelling sites on the RNAP are marked with a red star (satellites) and an exemplary labelling site on the DNA is marked with a green star (antenna). SmFRET measurements between satellite and antenna dyes are indicated with dotted beige arrows (B) Schematic representation of the global FRET network used to solve the complete architecture of the archaeal PIC. The unknown antenna positions (green circles) on the transcription factors as well as on the downstream, upstream and melted DNA region and the five known satellite sites on the archaeal RNAP (red circles) are shown together with the corresponding attached dyes (A647=Alexa 647; A555=Alexa555; Dl550=DyLight550; Dl650=DyLight650). FRET efficiencies were measured between pairs of satellite (acceptor) and antenna (donor) dyes (dotted black lines) and in between antennas (dotted red lines). In case of the latter measurements, one of the antenna positions had to be labelled with an acceptor, as indicated.*

Figure 2 Simulation results of the different model assumptions. *All pictures show the front view of the archaeal RNA polymerase (pdb ID: 2WAQ) together with the model for promoter DNA (tDNA and ntDNA in blue and cyan, respectively), TBP (purple), TFB (green) and TFE (yellow) in the archaeal PIC. Superimposed are the credible volumes for NPS simulation results of (**A**) the classic model, (**B**) the iso model, (**C**) the meanpos-iso model, (**D**) the var-meanpos-iso model and (**E**) the var-meanpos model. All volumes are shown at 68 % credibility. Comparing the credible volumes from the different models one finds that the size of the volumes strongly depends on the model used. Moreover, one also observes a shift of the position of the volumes upon introduction of a fixed mean position (**C**). Comparison of (**A**) and (**E**) as well as (**B**) and (**D**) shows that the change from a free static position to a free mean position has only a minor effect upon the size of the volumes, whereas the introduction of isotropic averaging leads to a large reduction of the volume ((**A**) and (**B**), (**D**) and (**E**)).*

Figure 3: Cartoon representation of different dye models used in NPS analysis. (A) *NPS is based on data from different smFRET measurements between dye molecules attached to different positions on the protein. Due to the flexible linkers used, the dye molecules may reside anywhere within their accessible volumes (AVs).* ***(B)*** *Classic model. Within the AV the dye molecule occupies one unknown position. At this position, the dye molecule can rotate, however, free rotation is only possible within a cone, whose size is determined from the respective fluorescence anisotropy. The orientation of the cone is not known leading to large uncertainties in the conversion from FRET efficiency to distance****. (C)*** *Iso model. The dye molecule resides at a fixed, yet unknown position within the AV. The fluorescence anisotropy is sufficiently small that dynamical averaging over all orientations is allowed****. (D)*** *Var-meanpos-iso model.. The position of the dye molecule is not fixed, instead the molecule moves about the AV; however, all positions are occupied equally, so that the center of the AV volume, the so-called mean position, can be used in the analysis, together with a polynomial correction accounting for the R^6-law of energy transfer. At each of the positions the dye molecule is free to rotate.* ***(E)*** *Var-meanpos-iso. Like Model 3 with the only difference that the mean positions of the dye molecule is not known, but needs to be determined by the*

experiment. ***(F)*** *Like the classic model, with the difference that the dye molecule dynamically switches between different positions resulting in a dynamically averaged mean position.*

Figure 4: Comparison of the size of credible volumes for the different models*. Compared are the computed credible volumes enclosing 68 %* ***(A)*** *and 95 %* ***(B)*** *of the probability. Data is visualized by boxplots. The blue box contains the inner 50 % of the data points, whereas the upper and lower bars, also called whiskers, represent the highest or lowest data points, respectively, still being in the 1.5 interquartile range, which is the length of the box in y-direction. Red crosses represent outliers, defined by not being in the 1.5 interquartile range, and the red line inside the box depicts the median. The inner boxplot is a zoom since the respective volumes are too small to be compared quantitatively on the same scale.*

Figure 5: Overlap of credible volumes between different models. *In order to investigate the overlap of credible volumes of different models, we computed credible volumes at increasing probability to test when one observes the first voxel that is common to the credible volumes of different models. The data is plotted as a function of the fluorescence anisotropy of the respective ADMs in order to test the isotropic orientation hypothesis. The credibility volumes at the first voxel overlaps between the var-meanpos model and the var-meanpos-iso model (red dots) and between the var-meanpos model and the meanpos-iso model (dark blue dots) are shown for the respective dyes. When comparing the meanpos-iso model overlap occurs only at values as high as 98 %, suggesting that the assumptions of the model are very unlikely for some dyes (e.g. nt(-24) or TBP-S71), because the assumed satellite state is also possible in the var-meanpos model. Additionally, we plotted arrows indicating the shift upon the introduction of a fixed mean position (switch from the var-mean-iso model to the meanpos-iso model). When looking at the data we found that the anisotropies of dye molecules attached to TFB and TBP were substantially higher than the other anisotropies; therefore, we used green arrows for describing localisations that used measurements to TBP and/or TFB and black arrows for all other localisations. Green arrows are generally much larger than black arrows suggesting that the assumption of a fixed mean position with respect to the accessible volume (AV) might not be valid here.*

Notes and references

‡ The developed Fast-NPS software package can be downloaded from http://www.uni-ulm.de/nawi/nawi-biophys/software.html.

1. P. Cramer, *Cell*, 2014, **159**, 985–994.
2. T. Schmeing and V. Ramakrishnan, *Nature*, 2009, **461**, 1234–1242.
3. K.-P. Hopfner and J. Michaelis, *Current Opinion in Structural Biology*, 2007, **17**, 87–95.
4. J. Menetrey, A. Bahloul, A. L. Wells, C. M. Yengo, C. A. Morris, H. L. Sweeney, and A. Houdusse, *Nature*, 2005, **435**, 779–785.
5. T. Ha, *Nat Meth*, 2014, **11**, 1015–1018.
6. L. Stryer and R. P. Haugland, *Proc Natl Acad Sci USA*, 1967, **58**, 719–726.
7. J. Michaelis, in *Single Particle Tracking and Single Molecule Energy Transfer*, Wiley-VCH Verlag GmbH & Co. KGaA, Weinheim, Germany, 2009, pp. 191–214.
8. I. Rasnik, S. Myong, W. Cheng, T. M. Lohman, and T. Ha, *J Mol Biol*, 2004, **336**, 395–408.
9. M. Margittai, J. Widengren, E. Schweinberger, G. F. Schröder, S. Felekyan, E. Haustein, M. König, D. Fasshauer, H. Grubmüller, and R. Jahn, *Proc Natl Acad Sci USA*, 2003, **100**, 15516–15521.
10. J. Andrecka, R. Lewis, F. Brückner, E. Lehmann, P. Cramer, and J. Michaelis, *Proc Natl Acad Sci USA*, 2008, **105**, 135–140.
11. N. K. Lee, A. N. Kapanidis, Y. Wang, X. Michalet, J. Mukhopadhyay, R. H. Ebright, and S. Weiss, *Biophys J*, 2005, **88**, 2939–2953.
12. R. E. Dale, J. Eisinger, and W. E. Blumberg, *Biophys J*, 1979, 1–33.
13. J. J. Mccann, U. B. Choi, L. Zheng, K. Weninger, and M. E. Bowen, *Biophys J*, 2010, **99**, 961–970.
14. A. Muschielok, J. Andrecka, A. Jawhari, F. Brückner, P. Cramer, and J. Michaelis, *Nat Meth*, 2008, **5**, 965–971.
15. A. Muschielok and J. Michaelis, *J Phys Chem B*, 2011, **115**, 11927–11937.
16. J. Andrecka, B. Treutlein, M. A. I. Arcusa, A. Muschielok, R. Lewis, A. C. M. Cheung, P. Cramer, and J. Michaelis, *Nucleic Acids Res*, 2009, **37**, 5803–5809.
17. B. Treutlein, A. Muschielok, J. Andrecka, A. Jawhari, C. Buchen, D. Kostrewa, F. Hög, P. Cramer, and J. Michaelis, *Mol Cell*, 2012, **46**, 136–146.
18. D. Grohmann, J. Nagy, A. Chakraborty, D. Klose, D. Fielden, R. H. Ebright, J. Michaelis, and F. Werner, *Mol Cell*, 2011, **43**, 263–274.
19. J. Nagy, D. Grohmann, A. C. M. Cheung, S. Schulz, K. Smollett, F. Werner, and J. Michaelis, *Nature Communications*, 2015, **6**, 6161.
20. J. Michaelis and B. Treutlein, *Chem. Rev*, 2013, **113**, 8377–8399.
21. S. Kalinin, T. Peulen, S. Sindbert, P. J. Rothwell, S. Berger, T. Restle, R. S. Goody, H. Gohlke, and C. A. M. Seidel, *Nat Meth*, 2012, **9**, 1218–1225.
22. S. Sindbert, S. Kalinin, H. Nguyen, A. Kienzler, L. Clima, W. Bannwarth, B. Appel, S. Müller, and C. A. M. Seidel, *J Am Chem Soc*, 2011, **133**, 2463–2480.
23. U. B. Choi, P. Strop, M. Vrljic, S. Chu, A. T. Brunger, and K. R. Weninger, *Nat Struct Mol Biol*, 2010, **17**, 318–324.
24. R. V. Craiu and J. S. Rosenthal, *Annual Review of Statistics and Its Application*, 2014, **1**, 179–201.
25. R. Swendsen and J. Wang, *Phys Rev Lett*, 1986, **57**, 2607–2609.
26. C. J. Geyer, *Statistical Science*, 1992.
27. A. Kone and D. A. Kofke, *J Chem Phys*, 2005, **122**, 206101.